

# A microfluidic refractometric sensor based on gratings in optical fibre microwires

Fei Xu,<sup>1</sup> Gilberto Brambilla,<sup>2</sup> and Yanqing Lu<sup>1</sup>

<sup>1</sup>Department of Materials Science and Engineering and National Laboratory of Solid State Microstructures, Nanjing University, Nanjing 210093, P. R. China

<sup>2</sup>Optoelectronics Research Centre, University of Southampton, Southampton, SO17 1BJ, United Kingdom

**Abstract:** In this paper we investigate a novel method to manufacture gratings in optical fiber microwires and discuss their application to sensing. Gratings can be manufactured by wrapping an optical fiber microwire on a microstructured rod. This method avoids post-processing the thin optical fiber microwire and it has great flexibility: chirping can be realized by designing the air hole size and position in the microstructured rod. By exploiting the large evanescent field in an inner channel, microfluidic refractometric sensors with sensitivity  $> 10^3$  nm/RIU can be achieved.

©2009 Optical Society of America

OCIS codes: (060.3735) Fiber Bragg gratings; (060.2340) Fiber optics components.

---

## References and links

1. G. Brambilla, V. Finazzi, and D. Richardson, "Ultra-low-loss optical fiber nanotapers," *Opt. Express* **12**(10), 2258–2263 (2004).
2. L. Tong, R. R. Gattass, J. B. Ashcom, S. He, J. Lou, M. Shen, I. Maxwell, and E. Mazur, "Subwavelength-diameter silica wires for low-loss optical wave guiding," *Nature* **426**(6968), 816–819 (2003).
3. A. M. Clohessy, N. Healy, D. F. Murphy, and C. D. Hussey, "Short low-loss nanowire tapers on singlemode fibres," *Electron. Lett.* **41**(17), 954–955 (2005).
4. K. O. Hill, Y. Fujii, D. C. Johnson, and B. S. Kawasaki, "Photosensitivity in optical fiber waveguides: Application to reflection filter fabrication," *Appl. Phys. Lett.* **32**(10), 647–649 (1978).
5. V. Hodzic, J. Orloff, and C. C. Davis, "Periodic Structures on Biconically Tapered Optical Fibers Using Ion Beam Milling and Boron Implantation," *J. Lightwave Technol.* **22**(6), 1610–1614 (2004).
6. D. Grobncic, S. J. Mihailov, C. W. Smelser, M. Becker, and M. W. Rothhardt, "Femtosecond laser fabrication of Bragg gratings in borosilicate ion-exchange waveguides," *IEEE Photon. Technol. Lett.* **18**(13), 1403–1405 (2006).
7. J. C. Knight, "Photonic crystal fibres," *Nature* **424**(6950), 847–851 (2003).
8. M. Bayindir, F. Sorin, A. F. Abouraddy, J. Viens, S. D. Hart, J. D. Joannopoulos, and Y. Fink, "Metal-insulator-semiconductor optoelectronic fibres," *Nature* **431**(7010), 826–829 (2004).
9. G. Brambilla, F. Xu, and X. Feng, "Fabrication of optical fibre nanowires and their optical and mechanical characterisation," *Electron. Lett.* **42**(9), 517–519 (2006).
10. W. Streifer, D. Scifres, and R. Burnham, "Coupling coefficients for distributed feedback single- and double-heterostructure diode lasers," *Quantum Electronics, IEEE Journal of* **11**(11), 867–873 (1975).
11. W. Streifer, and A. Hardy, "Analysis of two-dimensional waveguides with misaligned or curved gratings," *Quantum Electronics, IEEE Journal of* **14**(12), 935–943 (1978).
12. C. Y. Chao, and L. J. Guo, "Design and optimization of microring resonators in biochemical sensing applications," *J. Lightwave Technol.* **24**(3), 1395–1402 (2006).
13. S. Campopiano, R. Bernini, L. Zeni, and P. M. Sarro, "Microfluidic sensor based on integrated optical hollow waveguides," *Opt. Lett.* **29**(16), 1894–1896 (2004).
14. I. M. White, H. Oveys, and X. Fan, "Liquid-core optical ring-resonator sensors," *Opt. Lett.* **31**(9), 1319–1321 (2006).
15. M. Sumetsky, R. S. Windeler, Y. Dulashko, and X. Fan, "Optical liquid ring resonator sensor," *Opt. Express* **15**(22), 14376–14381 (2007).
16. A. Bernardi, S. Kiravittaya, A. Rastelli, R. Songmuang, D. J. Thurmer, M. Benyoucef, and O. G. Schmidt, "On-chip Si/SiO<sub>2</sub> microtube refractometer," *Appl. Phys. Lett.* **93**(9), 094106 (2008).
17. V. Zamora, A. Díez, M. V. Andrés, and B. Gimeno, "Refractometric sensor based on whispering-gallery modes of thin capillaries," *Opt. Express* **15**(19), 12011–12016 (2007).
18. M. Hee-Jong, P. Gun-Woo, L. Sang-Bum, A. Kyungwon, and L. Jai-Hyung, "Waveguide mode lasing via evanescent-wave-coupled gain from a thin cylindrical shell resonator," *Appl. Phys. Lett.* **84**(22), 4547–4549 (2004).
19. F. Xu, P. Horak, and G. Brambilla, "Optical microfiber coil resonator refractometric sensor," *Opt. Express* **15**(12), 7888–7893 (2007).

## 1. Introduction

Optical devices based on silica optical fiber microwires (OFM) have attracted increasing attention because of the recent developments in the fabrication technology [1–3]. OFM devices fabricated from sub-wavelength fibers offer several prospective benefits as compared to micro-phonic devices based on other principles; these include low insertion loss, complete fiber compatibility and flexibility. Being fabricated from a single-mode fiber, OFM devices do not experience any input/output coupling problem. Recently some devices have been realized with sub-wavelength OFMs, including OFM resonators which have been investigated intensively both theoretically and experimentally. Yet, there is much difficulty in manufacturing OFM gratings. The standard use of photosensitive fiber core and UV writing is inconvenient for a micrometer scale fiber taper due to the disappearance of the germanium core [4] and the decrease of the field overlap with the core. Alternative techniques, such as etching the standard fiber, focused ion beam milling or implantation [5], and femtosecond infrared irradiation [6] have been reported, although the last two methods managed to produce only third-order gratings.

In this Letter, we present a novel design to obtain gratings and chirped gratings in OFMs without post-processing: large chirps can be easily realized by designing a specific support rod. This device is very compact and can be coated and used as a sensor with large evanescent field in an inner fluidic channel. This effect can be exploited to design a microfluidic refractometric sensor with extremely high sensitivity.

## 2. Schematic of the grating structure

OFM gratings can be obtained by wrapping OFMs on microstructured rods, and then coating them with a low-loss polymer. The microstructured rod can be a thick microstructured fiber or it can be obtained by etching a cane used in the manufacture of microstructured fibres. Combining current enabling technologies on microstructured optical fibers [7, 8] and OFMs [9], it is possible to induce periodic or variable corrugations leading to the coupling between forward and backward propagating waves. The final OFM grating structure is shown in Fig. 1(a): it is a compact and robust micro-device with some air holes arranged in a circle. The mode propagating in the OFM experiences refractive index corrugations because its evanescent field overlaps with the support rod where there is alternation of glass and air holes. Here we only consider one ring of air holes; the inner large hole is also filled with air and the OFM is assumed perpendicular to the rod. When a coordinate increasing along the microfiber is used, the surface corrugations experienced by the mode propagating along the curvilinear coordinate are similar to those experienced by a mode propagating straight in proximity of a conventional planar grating. Unfolding the OFM, the OFM grating can be taken as a coated OFM on a planar substrate with air-hole corrugations: the equivalent structure is shown in Fig. 1 (b).

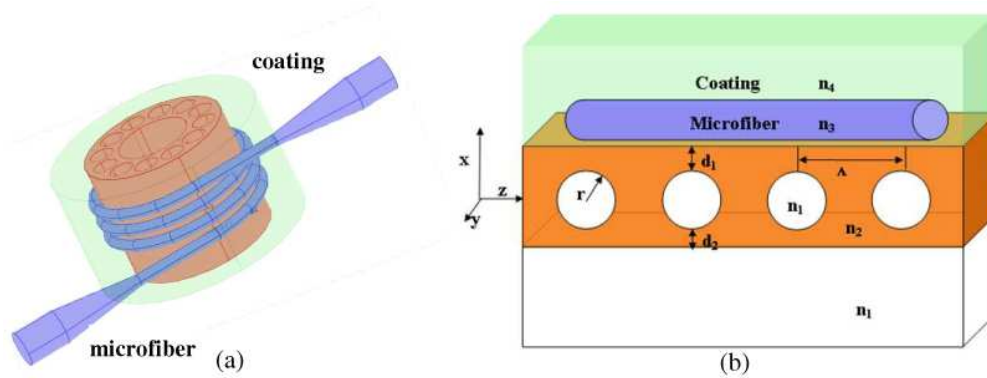


Fig. 1. (a) Schematic of the embedded OFM grating. (b) The equivalent planar structure;  $n_1, n_2, n_3, n_4$  are the refractive indexes of the hole, the rod, the OFM, and the coating, respectively;  $\Lambda$  is the distance between two adjacent holes;  $d_1$  and  $d_2$  are the thickness of the outer and inner walls of the one-ring microstructured rod,  $r$  is the hole radius.

As in other planar Bragg gratings and DFB lasers, the Bragg wavelength of the OFM grating is expressed by  $\lambda_B = 2n_{eff}\Lambda/m$  where  $n_{eff}$  is the mode effective index in the unperturbed (coiled) geometry,  $\Lambda$  is the period between two air-holes and  $m$  is the Bragg order.

The mode field in the unperturbed waveguide geometry is derived from the perturbed (straight) geometry using the method developed by W. Streifer [10, 11]: boundary between materials is shifted to compensate for the different geometry. If  $g_1$  is the boundary between the materials with refractive indices  $n_1$  (air) and  $n_2$  (the rod material, generally silica) and  $g_2$  is the boundary between the materials with refractive indices  $n_4$  (coating) and  $n_2$ , a new  $g_0$  is chosen to match the volume of  $n_1$  material extending into region A (above  $g_0$ ) to the volume of  $n_2$  material extending into region 1 (below  $g_0$ ), as shown in Fig. 2(a). We introduce the effective distance  $d_{eff}$  between  $g_2$  and  $g_0$  as:

$$d_{eff} = g_1 + g_2 - g_0 = d_1 + d_2 + 2r - \pi r^2 / \Lambda \quad (1)$$

$d_{eff}$  increases for increasing  $d = d_1 + d_2$  and decreasing  $\Lambda$ .

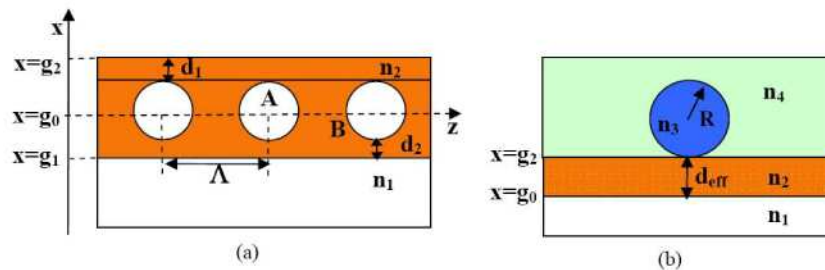


Fig. 2 (a) Illustration of the outer layer structure of the support rod in Streifer's theory.  $n_1$  and  $n_2$  represent the refractive indices of the hole and rod,  $\Lambda$  the distance between two adjacent holes,  $g_1$  and  $g_2$  the boundaries between different layers,  $g_0$  the new equivalent boundary between  $n_2$  and  $n_1$ . (b) The cross-section of the OFM in the equivalent outer straight layer structure,  $n_3$  and  $n_4$  are the index of the OFM and coating,  $R$  is the radius of the OFM and  $d_{eff}$  is the effective wall thickness

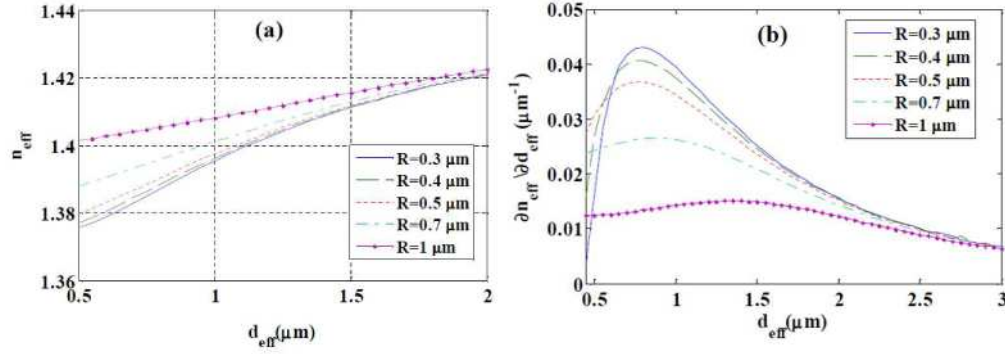


Fig. 3 (a) the effective index of OFM grating at different OFM radius depend on  $d_{eff}$  for  $n_1=1$ ,  $n_2=1.311$ ,  $n_3=1.451$ ,  $n_4=1.375$ , and  $\lambda=1550$  nm. (b)  $\partial n_{eff} / \partial d_{eff}$  depends on  $d_{eff}$  at different OFM radius.

The OFM cross-section in the equivalent outer straight layer structure is shown in Fig. 2 (b); in our simulations, the effective index and related propagation constant were obtained using the finite element method (FEM). Fig. 3(a) shows the dependence of the effective index on  $d_{eff}$  for different OFM radii at  $\lambda=1550$  nm.  $n_{eff}$  increases for increasing  $d_{eff}$  or  $R$ , as the OFM and rod have indices larger than that of the coating, and the mode is more confined in the microfiber when  $R$  increases or in the rod when  $d_{eff}$  increases.

This method to manufacture OFM gratings is extremely flexible: grating chirping can be achieved by tuning the hole radius and pitch, or by changing the distance between OFM and holes. Since  $\lambda=2n_{eff}(d_{eff})\Lambda/m$ , there are three simple ways to realize chirp: by tuning  $\Lambda$ ,  $d=d_1+d_2$ , and  $r$ . Chirp rates are defined as:

$$\begin{cases} \frac{\partial \lambda}{\partial d} = \frac{2}{m} \frac{\partial n_{eff}}{\partial d_{eff}} \Lambda \\ \frac{\partial \lambda}{\partial \Lambda} = \frac{2}{m} \frac{\partial n_{eff}}{\partial d_{eff}} \frac{\pi r^2}{\Lambda} + \frac{2}{m} n_{eff} \\ \frac{\partial \lambda}{\partial r} = \frac{2}{m} \frac{\partial n_{eff}}{\partial d_{eff}} (2\Lambda - 2\pi r) \end{cases} \quad (2)$$

All the derivatives  $\partial \lambda / \partial \Lambda$ ,  $\partial \lambda / \partial d$  and  $\partial \lambda / \partial r$  depend on  $\partial n_{eff} / \partial d_{eff}$ , which in turn is strongly dependent on  $d_{eff}$  and  $R$ . Fig. 3(b) shows that  $\partial n_{eff} / \partial d_{eff}$  is of the order of  $10^2 \mu\text{m}^{-1}$  and achieves the maximum at  $d_{eff} \sim 1 \mu\text{m}$ . For  $m=2$ , from Eq. (2)  $\partial \lambda / \partial \Lambda \gg \partial \lambda / \partial d \sim \partial \lambda / \partial r$ ; since  $\partial \lambda / \partial \Lambda > 1$ , chirped grating can be easily realized by tuning the grating period: current photonic crystal fiber (PCF) fabrication techniques make the low-cost period-tuning possible. Moreover,  $\partial \lambda / \partial d \sim \partial \lambda / \partial r \sim 10^{-5}$ : this is enough to produce small precise chirps in a simpler and cheaper way than inducing a temperature, strain or refractive-index gradients. If chirping is to be achieved simply by wrapping the OFM around the support rod, hole periodicity repeats itself after each OFM turn, thus the rod circumference limits the chirp length. However, OFM and microstructured rods allow for another method to achieve chirped gratings. If the OFM is not perpendicular to the rod (they cross at an angle  $\varphi$ ) the Bragg condition is expressed by [11]  $\lambda=2n_{eff}\Lambda/\cos\varphi/m$ ; by changing  $\varphi$  gradually, the Bragg wavelength will change gradually, too. Thus by gradually changing  $\varphi$  it is possible to control the grating Bragg wavelength and get a chirped grating. When  $\varphi$  is very small, the chirp rate is given by

$$\frac{\partial \lambda}{\partial \varphi} = -2 \frac{n_{eff} \Lambda \sin \varphi}{m \cos^2 \varphi} \sim 2 \frac{n_{eff} \Lambda \varphi}{m} = \Lambda \varphi \quad (3)$$

The chirp range varies considerably: from 0.3 nm/o at  $\varphi=0.1^\circ$  to 300 nm/o at  $\varphi=10^\circ$ .

These two chirping methods allow for a great deal of flexibility in the chirp design.

### 3. A refractometric sensor and its sensitivity

If the microstructured rod holes are used as microfluidic channels, the device shown in Fig. 1(a) can work as a refractometric sensor. The fluid can enter the microfluidic channels by capillarity. Because of the small hole size, extremely small fluid quantities are needed for the examination. Moreover, since only a very short piece of rod is needed for each device, the average device cost is very low. As a sensing device, the OFM is expected to have a considerable fraction of the power propagating in the evanescent field. Standard fiber gratings have thick claddings and this limits the extent of the evanescent field: they have to be post-processed (typically etching the cladding) to have a non-negligible fraction of power in the evanescent field. Moreover, a simple OFM has to be coated to avoid degradation [2] and this limits the extent of the evanescent field beyond the coating. On the contrary, OFM gratings can have a large evanescent field in an inner channel.

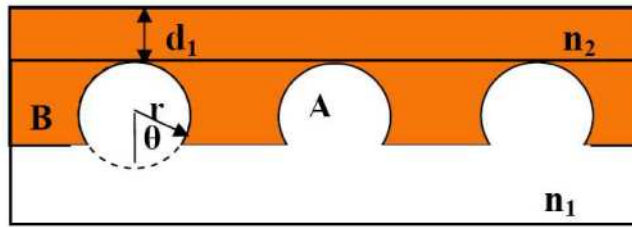


Fig. 4 Illustration of the outer layer structure of the support rod for  $d_2 < 0$ .

For sensing applications, large evanescent fields imply that  $d_1$  and  $d_2$  are expected to be as small as possible. Figure 4 shows that  $d_2$  can be negative ( $d_2 = -(r - r \cos \theta)$ ), thus:

$$d_{eff} = d_1 + r(1 + \cos \theta) - (r^2 / \Lambda)(\pi - \theta + \sin \theta \cos \theta). \quad (4)$$

$d_{eff}$  decreases when  $\varphi$  increases. A quantitative measurement of the sensor efficiency is given by the homogeneous sensitivity  $S$ , which can be obtained by monitoring the shift of the Bragg wavelength  $\lambda_B$  corresponding to a change in the analyte refractive index  $n_1$  [12]:

$$S = \frac{\partial \lambda}{\partial n_1} = \frac{\partial \lambda}{\partial n_{eff}} \frac{\partial n_{eff}}{\partial n_1} = \frac{\lambda}{n_{eff}} \frac{\partial n_{eff}}{\partial n_1} \quad (5)$$

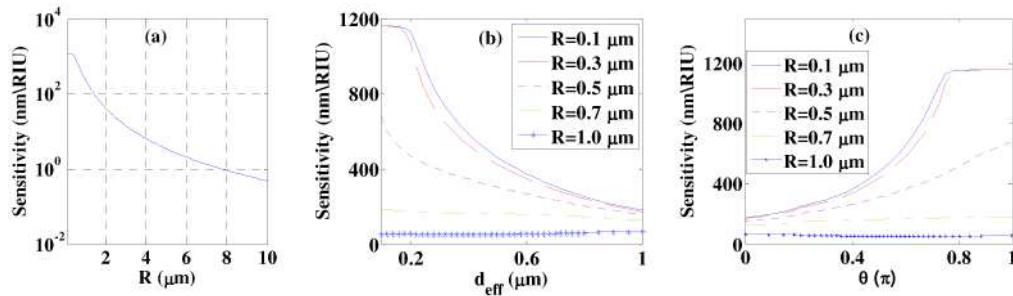


Fig. 5. (a) Dependence of the sensitivity  $S$  on OFM radius  $R$  for etched standard fiber gratings.  $n_f=1.332$  and  $\lambda=1550$  nm; (b) Dependence of  $S$  on  $d_{eff}$  for OFM gratings.  $n_f=1.332$ ,  $\lambda=1550$  nm and  $n_a=1.311$  (Teflon). (c) Dependence of  $S$  on  $\theta$  for OFM gratings,  $d_1=100$  nm,  $r=\Lambda/4$  and  $m=2$ .

Figure 5(a) shows the dependence of  $S$  on the OFM radius  $R$  for standard fiber Bragg gratings with etched cladding. Although  $S$  can achieve 1200 nm/RIU (where RIU is refractive

index unit) at  $R \sim 200$  nm, it is very difficult to get such a thin OFM by etching; generally, OFM manufactured by etching are several micrometers thick and  $S < 100$  nm/RIU in this range of diameters. Figure 5(b) shows the dependence of the sensitivity  $S$  on  $d_{\text{eff}}$  in OFM gratings:  $S$  increases for decreasing  $d_{\text{eff}}$  or  $R$ , because the fraction of the mode field inside the fluidic channel increases.  $S$  reaches 1200 nm/RIU at  $R \sim 200$  nm. The dependence of the sensitivity  $S$  on  $\theta$  is presented in Fig. 5(c): as before, because of the increased overlap between the mode propagating in the OFM and the microfluidic channel,  $S$  increases with  $\theta$ . Table 1 compares the sensitivity of several typical evanescent field microfluidic refractometric sensors: the sensitivity of OFM grating is the highest. Sensor 7 is made by wrapping an OFM on a soluble rod and its  $S$  can be close to that of an OFM grating sensor for  $R$  close to 300 nm, but it drops quickly with  $R$  and it reaches 20 nm/RIU for  $R \sim 1 \mu\text{m}$ . Sensor 8 is a typical etched fiber grating sensor:  $S \sim 100$  nm/RIU for  $R \sim 1.5 \mu\text{m}$  (Fig. 5(a)); however, it has major drawbacks: it has neither a fluidic channel to delivery the analyte nor the coating to protect itself from degradation; moreover, OFM is difficult to be etched to such a small size.

OFMs with diameters of several hundreds nanometres can be used in OFM grating:  $S$  can reach hundreds of nm/RIU, considerably better than that calculated for etched standard gratings (Fig. 5(a)). To achieve high sensitivity OFM grating sensors, negative  $d_2$  are required to easily achieve smaller  $d_{\text{eff}}$ . Although  $S$  increases for increasing  $\theta$ , the coupling strength decreases because the teeth depth is small.

**Table 1 . Sensitivity for evanescent field microfluidic refractometric sensors.**

	Type of sensor	Sensitivity nm/RIU	Reference	Notes
1	Integrated optical hollow waveguides	$\sim 555$	[13]	Wavelength 700nm
2	Liquid core optical ring resonator, Glass capillary and fiber taper	34	[14]	Wall thickness 2 $\mu\text{m}$
3	Optical liquid ring resonator, Coated glass capillary and fiber taper	$\sim 100$	[15]	Wall thickness 0
4	On-chip Si/SiOx microtube	$\sim 62$	[16]	
5	Thin capillaries	$\sim 100$	[17]	Wall thickness 0.8 $\mu\text{m}$
6	Thin Cylindrical shell resonator, polymer	$\sim 31.5$	[18]	
7	Optical fiber nanowire sensor	$\sim 1000$ $\sim 20$	[19]	OFM radius 300 nm OFM radius 1000 nm wavelength 1550 nm
8	Etched standard grating	$\sim 100$	[20]	Fiber radius: 1.5 $\mu\text{m}$
9	OFM grating	$\sim 1200$	This work	

#### 4. Conclusion

In conclusion, we have presented a novel method to manufacture gratings in OFM by wrapping an OFM on a microstructured rod. By designing microstructured rods with specific geometries or by changing the approach angle between microfiber and rod, grating chirping can be obtained. A refractometric sensor can be obtained exploiting the holes of the microstructured rod as microfluidic channels. The sensor sensitivity has been calculated and compared with other evanescent field refractometric sensors. OFM grating sensors can have extremely high sensitivity, in excess of  $10^3$  nm/RIU.

#### Acknowledgments

Gilberto Brambilla gratefully acknowledges the Royal Society (London, U.K.) for his research fellowship. Yan-qing Lu acknowledges the support from China MOE for new century and Changjiang scholars program. The authors acknowledge financial support by the UK EPSRC, China NSFC program under contract No. 60977039 and 10874080, and National 973/quantum manipulation program under contract No. 2006CB921805 and 2010CB327803. Gilberto Brambilla's and Fei Xu's e-mails are gb2@orc.soton.ac.uk and feixu@nju.edu.cn.